Structural Chemistry (2019) 30:1041–1055
https://doi.org/10.1007/s11224-018-1225-y

ORIGINAL RESEARCH

Interactions and physical properties of energetic poly-(phthalazinone ether sulfone ketones) (PPESKs) and ε-hexanitrohexaazaisowurtzitane (ε-CL-20) based polymer bonded explosives: a molecular dynamics simulations

Yao Shu[1] · Shaowen Zhang[1] · Yuanjie Shu[2] · Ning Liu[2] · Yong Yi[3] · Jichuan Huo[3] · Xiaoyong Ding[4]

Received: 4 October 2018 / Accepted: 2 November 2018 / Published online: 19 December 2018

Abstract

Molecular dynamic (MD) simulations were employed to investigate the hexanitrohexaazaisowurtzitane (CL-20) crystal, seven designed energetic poly-(phthalazinone ether sulfone ketones) (PPESKs) and PPESKs/ε-CL-20 polymer–bonded explosives (PBXs). Cohesive energy density (CED) and solubility parameters (δ) were predicted for PBXs, the results indicated that stability of PBXs are related to their cohesive energy density (CED). Mechanical properties of seven polymer-bonded explosives (PPESKs/ε-CL-20) were found improved in comparison with that of ε-CL-20 by adding polymer binders. Young's modulus (*E*), Shear modulus (*G*), and Bulk modulus (*K*) declined compare with ε-CL-20. *K*/*G* ratio and Cauchy pressure C_{12}-C_{44} of PBXs indicate that they have certain ductility. Radial distribution function (RDF) was utilized for analyzing the interactions between PPESKs and ε-CL-20, and results demonstrate that hydrogen bond and van der Waals interactions exist between polymers and ε-CL-20. The calculated oxygen balance of polymer-bonded explosives (PBXs) is lower than that of pure ε-CL-20 by nearly about − 24%. Detonation properties of the polymer-bonded explosives (PBXs) were predicted based on ε-CL-20 values. Detonation velocity (*D*) for these PBXs was predicted almost at about 8300 m s^{-1}, and the detonation pressure (*P*) for these PBXs was all predicted nearly at 38 GPa.

Keywords ε-CL-20 · PPESK · PBXs · Molecular dynamics · Binding energy · Mechanical property

Introduction

High energy and high security are generally two inconsistent properties for mono-explosives, and synthesis of low insensitive and high-energy density materials (HEDMs) has long been the purpose of scientists [1–3]. To date, hexanitrohexaazaisowurtzitane (CL-20) is one of the highest energy density material which can be available in practice (Fig. 1) [4–6]. CL-20 have four types of crystals at ambient conditions viz. the α-CL-20, the β-CL-20, the γ-CL-20, and the ε-CL-20 [7–10], and ξ-CL-20 crystal exists at 1.44 GPa [11]. The ε-CL-20 is the most stable type with the highest density among the five types. However, CL-20 is still restricted in practical applications, owing to its high expense and relatively high sensitivity under external stimuli. Therefore, how to minimize the sensitivity under external stimuli and make it more easily to be processed for CL-20 are two problems that need to be solved when it is extensively used in practice.

Electronic supplementary material The online version of this article (https://doi.org/10.1007/s11224-018-1225-y) contains supplementary material, which is available to authorized users.

✉ Shaowen Zhang
swzhang@bit.edu.cn

✉ Yuanjie Shu
1204172675@qq.com

[1] School of Chemistry and Chemical Engineering, Beijing Institute of Technology, Beijing 100081, China

[2] Xi'an Modern Chemistry Research Institute, Xi'an 710065, Shaanxi, China

[3] Southwest University of Science and Technology, Mianyang 621010, Sichuan, China

[4] Sichuan University of Science and Engineering, Zigong 643000, Sichuan, China

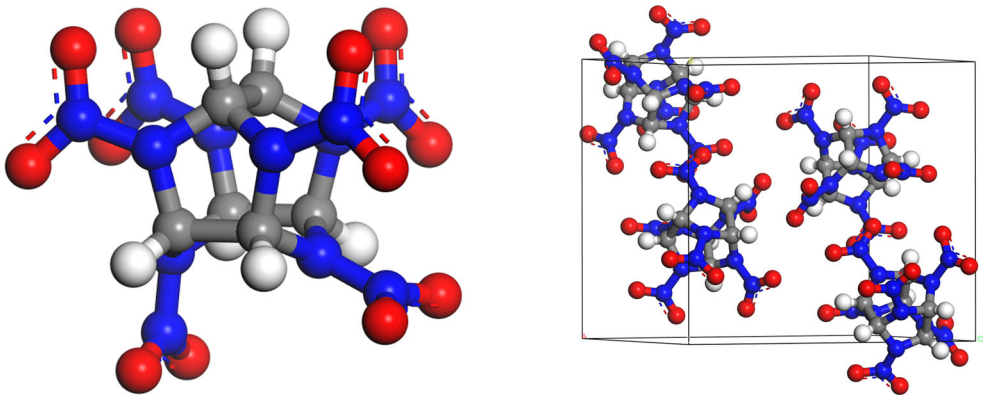

Fig 1 Molecular structure and primitive cell of the ε-CL-20 [12]

In recent years, several methods had been applied into increasing the stability of the ε-CL-20, such as crystallizing more stable co-crystals and forming polymer-bonded explosives (PBXs) [13–17]. Many calculations and experiments had been especially performed to investigate the CL-20 co-crystals, such as the CL-20/TNT [18], the CL-20/HMX [19, 20], the CL-20/Fox-7 [21], and the CL-20/DNP [22] co-crystals, and the results indicate that these CL-20 co-crystals are more stable than that of the pure CL-20; however, it is still infeasible for acquiring large amount of co-crystals. Polymer-bonded explosives (PBXs), containing 5–10 wt% polymer binders and 90–95 wt% [23, 24] energetic particles, are not only stable than mono-explosives, but also more easily available and processed than co-crystals. Some CL-20–based PBXs had been acquired in recent years by Zeman et al. [25, 26]; however, the new formula for PBXs is worth selecting for avoiding the danger of synthesis and consuming the time. Based on these reasons, some theoretical works have been operated previously. Yuan et al. [27] studied the mechanical properties and interactions of ε-CL-20–based PBX by using PEG and PVA as polymer binders via the MD simulations. The results implied that the PEG/ε-CL-20 PBXs were more stable than the PVA/ε-CL-20 PBXs, due to the higher binding energy of the former than that of the latter. The elasticity and the ductility of the PEG/ε-CL-20–based PBX were superior to that of the PVA/ε-CL-20–based PBX, owing to the side-chain of PEG which is more flexible than that of PVA. Tao et al. [28] investigated the interaction of the ε-CL-20–based PBXs by using different ratio segments for polymers (AMMO: BMMO). The results indicated that the stability of the PBXs were elevated by introducing the energetic binders, and as the segments AMMO were more added, the elasticity and the ductility of the PBXs were more superior.

Phazalazione (DHPZ)-contained polymers have good physical and mechanical properties, which have been applied into insulating material and composite materials [29, 30]. These kinds of polymers have high glass transition temperature (T_g) (usually above (500 K)) and good thermal stabilities, owing to the non-coplanar aromatic rings of DHPZ. Arising from the special structure of DHPZ, DHPZ-contained polymers have non-coplanar structures as well, which impede polymers to crystalize and make polymers prone to dissolve. In the recent two decades, Jian and his co-workers [31, 32] had synthesized a series of DHPZ-contained polymers, which not only have good physical and mechanical properties, but also endure high temperature and are easier to be dissolved than traditional polymers. However, these types of polymers have not yet been used as polymer binders in PBXs in practice, and only had been investigated preliminarily by Wang et al. with MD simulations [33]. They had designed energetic DHPZ polymers by introducing -NH_2 and -NO_2 into the polymer chains, and then they studied the interactions between polymers and different graphs of ε-CL-20 by molecular dynamics. Their study indicated that the rigidity of the PPESK/ε-CL-20 PBX was much lower than that of the pure ε-CL-20, and binding energy values of the PBXs were all positive, implying that these PBXs had good cohesive ability. We had designed several energetic PPESK polymers by introducing -NO_2,-NH_2,-ONO_2,-N_3, and -NF_2 functional groups into the polymer chains respectively in our previous work [34]. Physical and mechanical properties of these polymers had been predicted via molecular dynamic (MD) simulations. Meanwhile, the prediction results of these polymers indicated that the optimal ratio for sulfone and ketone segments were predicted to be 8:2, ascribing to its higher T_g values at this ratio [35]. Preliminary study had investigated PPESK (A and B (shown in Scheme 1))/TNT PBXs and PPESK (A and B)/TATB PBXs mechanical properties by MD simulations. The results illustrate that the rigidity of the PBXs were lower than that of the corresponding pure explosives. The binding energy of these PBXs was all positive, implying that the two composites (binders and explosives) had well combining capacity.

In this paper, we use designed energetic PPESKs (see Scheme 1) as polymer binders, ε-CL-20 as the main explosive, to investigate physical and mechanical properties of the PPESK (A-G)/ε-CL-20 PBXs. For simplicity, PPESK A/ε-CL-20PBX was abbreviated as PBX A, and other polymer-bonded explosives were similarly shortened as

Scheme 1 The designed PPESKs as polymer binders for ε-CL-20–based PBXs [34]

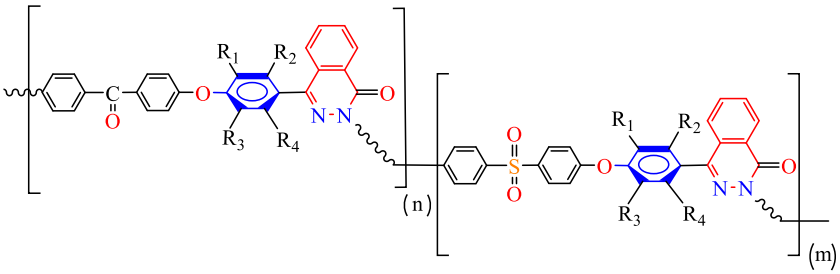

n:m=2:8

PPESK A $R_1=R_2=R_3=R_4=H$
PPESK B $R_1=NO_2$ $R_2=H$ $R_3=R_4=NH_2$
PPESK C $R_1=R_3=NO_2$ $R_2=R_4=H$
PPESK D $R_1=R_3=NH_2$ $R_2=R_4=H$
PPESK E $R_1=R_3=CH_2N_3$ $R_2=R_4=H$
PPESK F $R_1=R_3=CH_2ONO_2$ $R_2=R_4=H$
PPESK G $R_1=R_3=NF_2$ $R_2=R_4=H$

PBXs (B-G) according to the different polymer binders used in Scheme 1.

Models and methods

Primitive ε-CL-20 cell was cited from Cambridge Crystallographic Data Center (CCDC), and it belongs to the P21/n space group, with cell parameters a = 8.852 Å, b = 12.556 Å, c = 13.386 Å, α = γ = 90°, and β = 106.82 [12]. Based on the ε-CL-20 primitive cell, a 4 × 3 × 3 supercell was constructed, and it was then cleaved along the (0 0 1) crystal surface, owing to the fact that molecules on this crystal surface packed more tightly [36]. Thereafter, a 20-Å vacuum layer was added along the *z*-axis (c direction), and the constructed supercell consists of 144 molecules and 5184 atoms. Moreover, amorphous polymers were built by the Amorphous Cell (AC) module of the Material Studio software [37] and subsequently used as polymer binders. The AC module is a force-based tool based on the Monte Carlo methods to construct polymer configurations [38], and polymers were then optimized for subsequent molecular dynamic simulations. The optimized polymers were put into the vacuum to build PBX models, which were then constantly compressed and optimized for lowering energy of composites until the densities of PBXs got close to theoretical density. Constructed PBXs possess different atom numbers from 5674 to 5794 (specific numbers for corresponding PBXs is shown in Table 1).

Seven constructed PBXs (see Fig. 2) were firstly optimized to obtain the lowest energy, and their corresponding output configurations were then used for subsequent molecular dynamic simulations. Specific simulations for these PBXs were performed at the temperature of 298 K and the pressure of 10^5 Pa, and 2 ns ran for the total simulation by using the isobaric-isotherm (NVT) ensemble. Moreover, the temperature and the pressure were controlled by Anderson thermostat [39] and Barostat [40] methods, and the Ewald- and the Atom–based [41] methods were used for Electrostatic and van der Waals (vdW) for summation method; moreover, the cut-off distance was set as 1.55 nm, the spline width was 0.1 nm, and Buffer width was 0.05 nm, respectively. During the whole simulation, the time step was set as 1 fs, and after molecular dynamic simulations the last 200 ps data were collected for processing.

The COMPASS force filed [42] had been confirmed not only working well in MD simulations for energetic polymers and nitro-contained energetic complexes [32, 43], but also suitable for PBXs [44]. Thus, the COMPASS force filed was applied in whole optimizations, MD simulations, and property analysis for PBXs.

Results and discussions

Criteria of system equilibrium

Temperature and energy are two criteria of judging equilibrium of system. For temperature, fluctuations within 5% of assigned simulated temperature indicate that the system reached equilibrium. Namely, the difference of the temperature (simulated temperature is 298 K) is no more than ± 15 K. Similarly, the energy fluctuations are within 5% of the calculated energy as well, that is to say, the energy fluctuations are within subtle changes or around average values. Taking PBX A for example, Fig. 3 displays the fluctuation curves of temperature (Fig. 3(a)) and energy (Fig. 3(b)) in MD simulations of PPESK A on the molecule layers parallel to the (0 0 1) crystalline surface of ε-CL-20. It can be noted that the plot of temperature vs simulation time are between 285 K and 305 K, namely, the fluctuations of temperature are no more than 15 K.

Table 1 Atom numbers, polymer ratios, and densities of the PBXs (A–G) and ε-CL-20

Entry	PBX A	PBX B	PBX C	PBX D	PBX E	PBX F	PBX G	ε-CL-20
Atom numbers	5674	5734	5714	5714	5774	5794	5714	5184
Polymer ratio	6.8 wt%	7.7 wt%	7.9 wt%	7.1 wt%	8.1 wt%	8.7 wt%	8.0 wt%	–
ρ (g cm^{-1})	1.710	1.729	1.733	1.717	1.738	1.748	1.736	2.01

The energy of the PBX simulations contain three kinds of energy, viz. the total energy, the potential energy, and the non-bond energy, the plot of all these energies vs simulation time tend to be smooth. The temperature and energy equilibrium state for other PBXs can be seen in the Fig. S1 and they have similar situations as that of PBX A.

Polymer ratios and densities of the PBXs

Polymer ratios of the PBXs usually within the range of 5–10 wt%, if ratios are lower than 5 wt%, the mechanical properties of the PBXs would be drooped. Contrarily, if ratios are higher than 10 wt%, the energy release of the PBXs would be reduced. The atom numbers in polymers are different, leading to the different atom numbers of the PBXs. Some PBXs own the same atom numbers (PBX C, PBX D, and PBX G), but the different elements and the different atom mass lead to the discrepancy of polymer ratios of these PBXs. From Table 1, it can be found that all polymer binders in the PBXs are within the range 5–10 (wt%), meeting the requirement for polymers in PBXs. The polymer ratios follow the sequence as: 8.7 wt% (PBX F) > 8.1 wt% (PBX E) > 8.0 wt% (PBX G) > 7.9 wt% (PBX C) > 7.7 wt% (PBX B) > 7.1 wt% (PBX D) > 6.9 wt% (PBX A). Densities of the PBXs have been predicted and they are displayed in Table 1 as well, it can be found that the highest density is 1.748 g cm^{-1} (PBX F), with the -CH_2ONO_2 groups introduced into the polymers, and the lowest density is 1.710 g cm^{-1} (PBX A), which is with no functional groups introduced into this polymers. Densities of the PBXs (B-G) are all higher than that of PBX A, comparing with these values it can be found that these density vales are closely related to their ratios of polymers in PBXs, and their density values follow the sequence: 1.748 g cm^{-1} (PBX F) > 1.738 g cm^{-1} (PBX E) > 1.736 g cm^{-1} (PBX G) > 1.733 g cm^{-1} (PBX C) > 1.729 g cm^{-1} (PBX B) > 1.717 g cm^{-1} (PBX D) > 1.710 g cm^{-1} (PBX A).

Cohesive energy density (CED) and solubility parameter (δ)

Cohesive energy density (CED) and solubility parameters (δ) are two indications for the compounds solubility. CED is the amount of energy needed to remove the unit volume of molecules from their neighbors to infinite separation (an ideal gas) completely [45]. It is equal to the heat of vaporization of the compound divided by its molar volume in the condensed phase. Moreover, solubility parameter is acquired by the square root of CED values, and Eq. (1) displays the relationship of CED and δ, where V_m is the molar volume, ΔH_v is the enthalpy of dissolution,

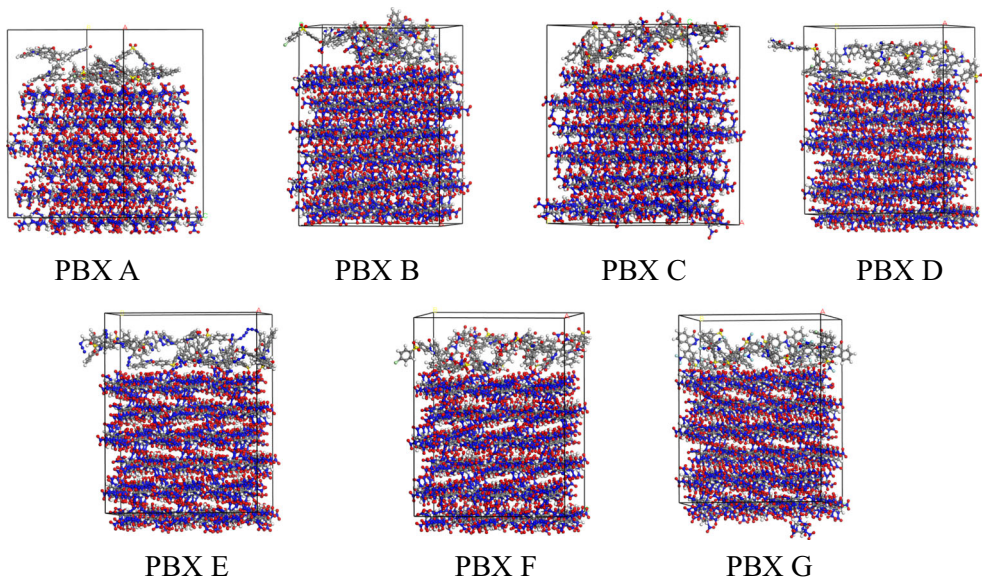

Fig. 2 Seven PBX models designed by polymer binders and ε-CL-20, in which C, N, O, S, H, and F(Cl) atoms display as gray, blue, red, yellow, white, and pale green beads

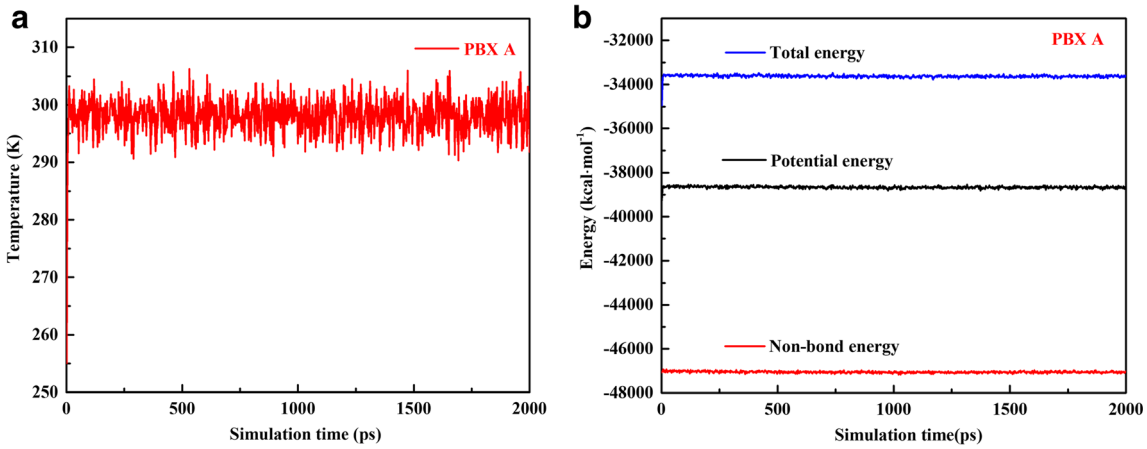

Fig. 3 Plot of temperature (**a**) and energy (**b**) vs. simulation time for PBX A via the PPESK A on ε-CL-20(100) crystalline surface at the temperature 298 K

ΔU_v is the heat of vaporization, R is the ideal gas constant, and T is the temperature. CED and δ of the designed polymer binders have been predicted in our previous work [34]. In this paper, we have predicted CED and δ of the PBXs to investigate the change of the solubility when the polymer binders were introduced into the CL-20 as displayed in Table 2. It can be found that the δ values follow the sequence as: 0.854 (kJ $cm^{-3})^{0.5}$ (PBX F) > 0.849 (kJ $cm^{-3})^{0.5}$ (PBX D) > 0.843 (kJ $cm^{-3})^{0.5}$ (PBX A) > 0.794 (kJ $cm^{-3})^{0.5}$ (PBX E) > 0.781 (kJ $cm^{-3})^{0.5}$ (PBX B) > 0.714 (kJ $cm^{-3})^{0.5}$ (PBX C) > 0.686 (kJ $cm^{-3})^{0.5}$ (PBX G). Since δ is obtained from the square root of the CED, CED has the same sequence for these PBXs as δ have. The results imply that PBX F and PBX D are harder to vaporize than the other PBXs, namely, they are more stable among the PBXs. On the contrary, PBX C and PBX G are more unstable among the PBXs because of their low CED values.

$$\begin{aligned} \Delta U_v &= \Delta H_v - RT \\ \mathrm{CED} &= \Delta U_v / V_m \\ \delta &= \sqrt{\Delta U_v / V_m} \end{aligned} \quad (1)$$

On the other hand, CED can be divided into two parts, namely, the van der Waals (vdW) energies (E_{vdW}) and the Electrostatic energies ($E_{Electrostatic}$), in which all $E_{Electrostatic}$ of PBXs are about 0.4 kJ cm^{-3}, indicating that ε-CL-20 have similar electrostatic interactions with different polymer binders. However, discrepancy of E_{vdW} values for PBXs indicate that there are different vdW interactions between polymer binders and ε-CL-20, which lead to the different cohesive energy density of polymers. Especially, the smaller E_{vdW} values of PBX G and PBX C indicate that the interactions between polymers (PPESK G and PPESK C) and ε-CL-20 are weaker, demonstrating that PBX G and PBX C are more unstable than other PBXs.

Pyrolytic trigger bond (N-NO_2) length

Discriminant sensitivity for HEDMs and crystals had been reported in previous reports [46], but it is difficult for PBXs and other composited energetic materials because of their complex systems. To investigate ε-CL-20 sensitivity influenced by introducing polymer binders in PBXs, the simple way is to assess the bond length of the PBXs by MD simulations, for the bond length and the bond order are closely related to strength of the chemical bond. That is to say, if the bond length were obtained, the relative strength of chemical bond could be estimated. Generally, the bond length of N-NO_2 is usually considered as the pyrolytic trigger bond in ε-CL-20, and they are considered as the key initiate for explosion as well. Though the bond order of the N-NO_2 bond are unable to obtain by MD simulations, the changes of the bond length are feasible to acquire, and thus the stability of the PBXs can be further predicted via the bond length. Table 3 shows the N-NO_2 bond lengths of ε-CL-20 in seven PBXs, in which L_{ave} is the average bond length of N-NO_2 in ε-CL-20–based PBXs,

Table 2 CED and δ of PBXs and ε-CL-20

	PBX A	PBX B	PBX C	PBX D	PBX E	PBX F	PBX G	ε-CL-20
CED (kJ cm^{-3})	0.71	0.61	0.51	0.72	0.63	0.73	0.47	0.93
E_{vdW} (kJ cm^{-3})	0.31	0.20	0.08	0.31	0.21	0.31	0.07	0.38
$E_{Electrostatic}$ (kJ cm^{-3})	0.40	0.41	0.43	0.41	0.42	0.42	0.40	0.55
δ (kJ $cm^{-3})^{0.5}$	0.843	0.781	0.714	0.849	0.794	0.854	0.686	0.964

Table 3 Three types of bond length of -N-NO_2 in ε-CL-20–based PBXs (Å)

	ε-CL-20	PBX A	PBX B	PBX C	PBX D	PBX E	PBX F	PBX G
L_{ave}	1.39	1.39	1.40	1.43	1.40	1.39	1.39	1.39
L_{prob}	–	1.39	1.39	1.39	1.39	1.39	1.39	1.39
L_{max}	–	1.41	1.41	1.49	1.41	1.41	1.41	1.41

L_{prob} is the probable bond length of N-NO_2 in ε-CL-20–based PBXs, and L_{max} is the maximum bond length of N-NO_2 in ε-CL-20–based PBXs. It can be found that the bond length of N-NO_2 has changed more or less in ε-CL-20–based PBXs compared to that of the pure ε-CL-20. L_{ave} values of N-NO_2 in ε-CL-20–based PBXs are 1.39 Å except for PBX B (1.40 Å), PBX C (1.43 Å), and PBX D (1.40 Å). All L_{prob} values of N-NO_2 in ε-CL-20–based PBXs are 1.39 Å, same as that in pure ε-CL-20. Nevertheless, L_{max} is considered as pyrolytic trigger bond in ε-CL-20 of PBXs, the largest N-NO_2 bond length is 1.49 Å (PBX C) and other N-NO_2 bond lengths are all equal to 1.41 Å, which are slightly longer than the N-NO_2 bond length in pure ε-CL-20. That is to say, PBX C is the most unstable PBX owing to its largest L_{max} N-NO_2 length bond at room temperature. In general, from these three kinds of N-NO_2 bond length in ε-CL-20–based PBXs, it can be found that these bond length values are similar or higher than that in pure ε-CL-20.

Binding energy

The binding energy (E_{bind}) is regarded as the determining criteria of interactions between different surfaces of various composites, and it is commonly defined as negative interaction energies (E_{inter}) [47]. If the E_{bind} values were positive and higher, the strength of the interactions between the two component surfaces of the composite would be stronger. The E_{inter} energy is obtained by the total energy of composite to subtract the sum of separate energies. Owing to the different PBXs with the different polymer ratios, using E_{bind} to assess the surface interactions of the two components for different PBXs might be irrational, thus, it might be reasonable that the E^* as 1 wt% polymer ratio of the E_{bind} for all PBXs is introduced to evaluate the surface interactions of the two components. Eq. (2) displays the relationships of the E_{bind}, the E_{inter}, the total energy of PBXs, and the energies of PBX components. In Eq. (2), E_{PBX} is the total energy of the PBX, E_{Poly} is the energy of polymer binder with ε-CL-20 eliminated from the PBX and $E_{ε\text{-}CL\text{-}20}$ is the energy of ε-CL-20 with the polymer subtracted from the PBX. Seven PBXs' binding energies are obtained at 298 K, and specific values can be seen in Table 4**.** It can be noted that E^* values of PBX G, PBX C, and PBX B are negative, demonstrating that their corresponding polymer binders cannot cohere with ε-CL-20 well, leading to weak interactions between the surface of polymer and the ε-CL-20 (0 0 1) surface. Other four PBXs' E^* values are all positive, in which the maximum value is 41.82 kcal mol^{-1} (PBX E), implying that the interaction between the PPESK E and ε-CL-20 (0 0 1) is stronger than that of the other PPESKs. Based on E^* values, stability of these PBXs follow the sequence as: PBX E > PBX F > PBX D > PBX A > PBX G > PBX B > PBX C.

$$E_{bind} = -E_{inter} = -\left(E_{PBX} - E_{Poly} - E_{\varepsilon-CL-20}\right) \quad (2)$$

Radial distribution function (RDF) analysis

Radial distribution function (RDF) is used to analyze the interactions of different composites; it measures the probability of certain atom appearing at a distance r from the designated atom. The $g(r)$-r relations of PBX A are displayed in Fig. 4 and other PBXs' $g(r)$-r relations are shown in Fig. S2. Moreover, the specific name of atoms described in $g(r)$-r relation figures is denoted as follow: (a) N, O, and H atoms in ε-CL-20 labeled as N_1, O_1, and H_1, respectively; (b) N, H, O, and F atoms in polymers labeled as N_2, H_2, O_2, and F_2, respectively. In addition, since the function groups have been introduced into the polymers, the influence of interactions between the polymers and the ε-CL-20 is various. Thus,

Table 4 Binding energies of PBXs with their corresponding polymers on ε-CL-20 (0 0 1) surface at 298 K (kcal mol^{-1})

	PBX A	PBX B	PBX C	PBX D	PBX E	PBX F	PBX G
	− 43,820.68	− 41,530.92	− 39,740.91	− 43,369.84	− 42,188.81	− 44,116.91	− 39,301
E_{Poly}	3922.77	4337.8	4163.37	4391.07	5609.95	3701.53	4403.08
$E_{ε\text{-}CL\text{-}20}$	− 47,580.8	− 47,366.02	− 47,518.25	− 47,584.66	− 47,460.02	− 47,530.31	− 47,551.5
E_{inter}	− 162.62	1497.3	3613.97	− 176.25	− 338.74	− 288.13	820.11
E_{bind}	162.62	− 1497.3	− 3613.97	176.25	338.74	288.13	− 820.11
E^*	23.91	− 194.4	− 457.46	24.82	41.82	33.12	− 102.51

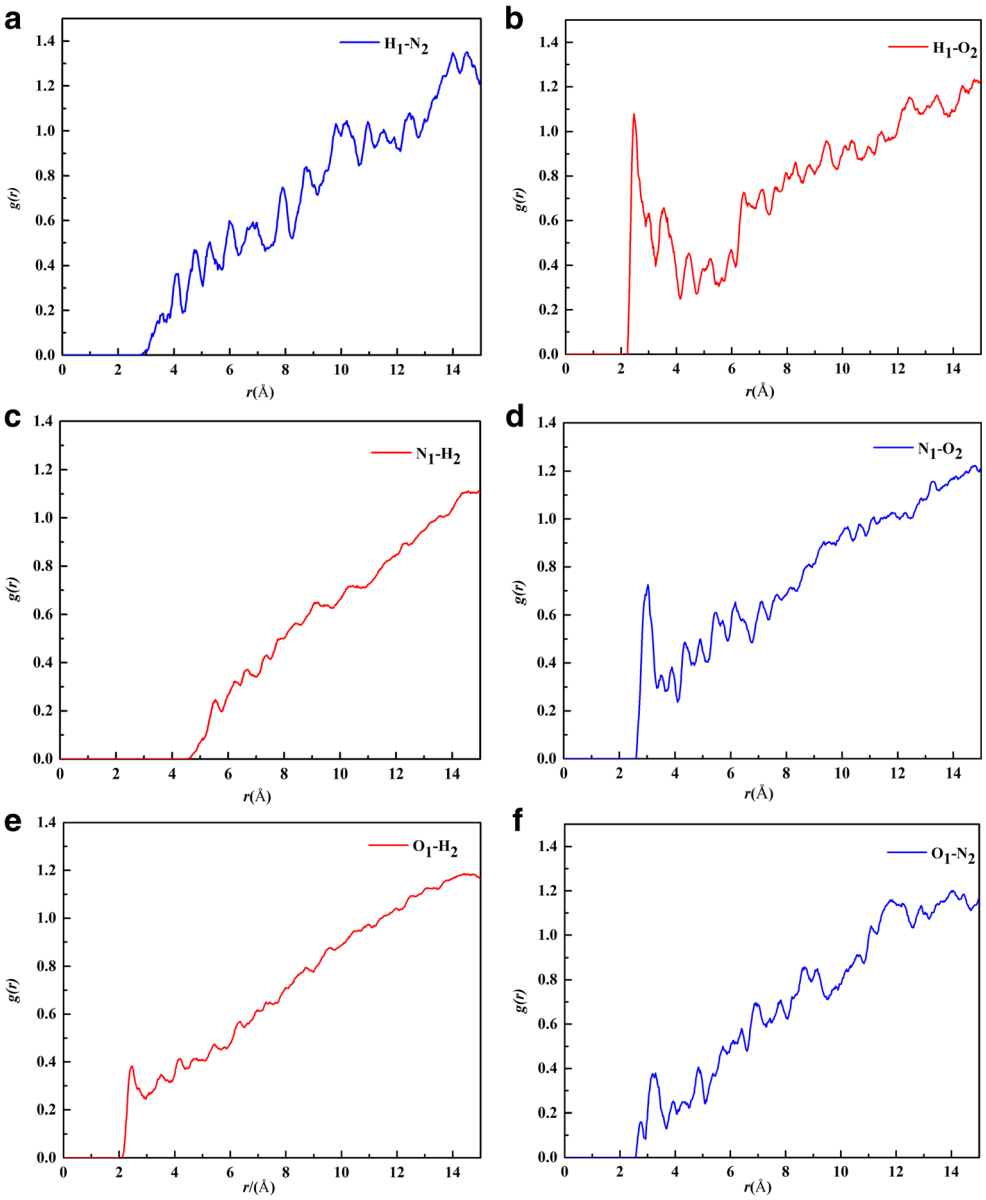

Fig. 4 Radial distribution function of PPESK A/ε-CL-20 (0 0 1) PBX

contributions of the introduced function groups are considered in *g(r)-r* relations, that is to say, N_2, O_2, and H_2 atoms from introduced function groups and polymers are separately considered for assessing each of their contributions in *g(r)-r* relations.

Generally, intermolecular interactions consist of hydrogen bond interactions and van der Waals (vdW) force. Moreover, vdW force can be further divided into dipole-dipole, induction and dispersion forces. If the distance *r* of two atoms is in the ranges of 2.6–3.1 Å, 3.1–5.0 Å, or above 5.0 Å, the interactions between them can be ascribed into the hydrogen bond interactions, the strong vdW force, or the feeble vdW force, respectively. Though hydrogen bond interactions are weaker than chemical bond, it is still the strongest force among the intermolecular interactions.

From Fig. 4(a), it can be found that H atoms from ε-CL-20 have no hydrogen bond interactions with N atoms from PPESK A during the distance range 2.6–3.1 Å, and at 4.1 Å and 4.8 Å, the *g(r)* values are 0.36 and 0.46, respectively, indicating that there are weak vdW forces between these two types of atoms. During the distance range 2.6–3.1 Å (Fig. 4(b)), a relatively high peak appears in *g(r)* (1.0) between the H_1-O_2 interaction, predicting that they have strong hydrogen bond interactions. Two moderate peaks are in the range of 3.1–5.0 Å, predicting that medium intensity of strong vdW force exists between the H_1-O_2 atom pairs. Figure 4(c) displays that no hydrogen bond interactions and strong vdW force between the N_1-H_2 atom pairs. In the range of 3.1–5.0 Å, a comparative high peak in *g(r)* of the N_1-O_2 atom pairs (Fig. 4(d)) predicts that strong vdW force exists between the

N_1 and O_2 atoms. As seen from Fig. 4(e), a small peak appearing at 2.45 Å, with weak intensity *g(r)* at 0.38, indicates that O_1-H_2 have small hydrogen bond interactions and vdW force. From Fig. 4(f), it can be noted that at 3.3 Å, there has a shoulder peak with *g(r)* = 0.37, implying that little strong vdW force exists between O_1 and N_2 atoms.

Additionally, since several function groups were introduced into the aromatic backbone of PPESK A, its interactions with ε-CL-20 may be different with that of PPESKs (B-G). Thus, how the function groups influence the properties of polymers and the interactions of polymers with ε-CL-20 need to be considered. To that end, the interactions of N, O, and F atoms from the introduced groups of polymers with ε-CL-20 also have been analyzed. Since there may exist hydrogen bond between the atom pairs H_1–N_2, N_1-H_2,H_1–O_2 and O_1–H_2 in other PBXs (PBX B to PBX G), all these pairs between the distance 2.6-3.1 Å in these PBXs have been taken into account. For the N_1-O_2 and O_1-N_2 atom pairs, their strong vdW interactions have been taken into account for other PBXs (PBX B to PBX G) as well. The H_1-N_2 atom pairs for PBX G (as shown in Fig. S2 PBX G (a)) has the lowest *g(r)* values nearly at 0.3 in the range of 2.6–3.1 Å. For PBX B and PBX F, their H_1-N_2 atom pairs (displayed in Fig. S2 PBX B (a) and PBX F (a)) have the *g(r)* values about 0.4 during the same range. Moreover, during the range of 2.6–3.1 Å, the H_1-N_2 atom pairs for PBX C, PBX D, and PBX E have the *g(r)* values more than 0.6. Analyzing the H_1-O_2, the N_1-H_2, and the O_1-H_2 for PBX B-PBXG (as shown in Fig. S2 PBX B(b)-PBX G(b), PBX B(c)-PBX G(c), and PBX B(e)-PBX G(e)) by the same way, it can be found that N_1-H_2 and O_1-H_2 have the weak hydrogen interactions ascribing to their *g(r)* values are less than 0.4 in the range of 2.6–3.1 Å. Besides, for H_1-O_2 atom pairs of the PBX B-PBX G, their *g(r)* values are more than 0.6, and even for PBX C, PBX D, and PBX F their *g(r)* values can be reached higher than 1.0 in the range of 2.6–3.1 Å. However, the N_1-O_2 and the O_1-N_2 atom pairs of PBX B-PBX G have less strong vdW interactions because of the low *g(r)* values in the range of 3.1–5.0 Å (as shown in Fig. S2 PBX B(d)-PBX G(d) and PBX B(f)-PBX G(f)).

So, based on these results, it can be found that H_1-O_2 atom pairs of PBX B-PBX G have the strongest hydrogen bond interactions because of the higher *g(r)* values in the range of 2.6–3.1 Å. The H_1-N_2, N_1-H_2, and O_1-H_2 atom pairs of PBX B-PBX G have low *g(r)* values (mainly about 0.4) in the range of 2.6–3.1 Å. Otherwise, the N_1-O_2 and the O_1-N_2 atom pairs of PBX B-PBX G have less strong vdW interactions due to their low *g(r)* values in the range of 3.1–5.0 Å. The RDF of the PBXs (PBX B-PBX G) have been divided into two or more parts and their contributions are displayed and colored in different lines in Fig. S2, respectively.

Mechanical properties

The symbols of σ and ε in Eq. (3) express the material stress and strain tensor, respectively. To statistical mechanics of elasticity, the generalized Hooke's law usually denoted as [48].

$$\sigma_i = C_{ij}\varepsilon_{ij} \ (i,j = 1,2,\ldots,6) \tag{3}$$

where C_{ij} is a 6 × 6 elastic coefficient matrix within 36 elastic constants as elements of the Matrix 5. Because of the property of strain energy and the symmetry of the matrix, that is $C_{ij} = C_{ji}$, thus, only 21 elastic constants are required for analyzing the stress and the strain properties of the materials. The elastic constants (see in the Table 5) can be classified as three groups, viz. C_{11},C_{22},C_{66}; C_{33},C_{44},C_{55}; and C_{12},C_{13},C_{23}; according to the closeness of values. Two parameters λ and μ are obtained by the C_{ij} elastic constants, and their relationships are displayed in Eq. (4).

$$\begin{aligned} \lambda &= \frac{1}{3}(C_{11}+C_{22}+C_{33}) - \frac{2}{3}(C_{44}+C_{55}+C_{66}) \\ \mu &= \frac{1}{3}(C_{44}+C_{55}+C_{66}) \end{aligned} \tag{4}$$

Table 5 Elastic constants of ε-CL-20 and designed PBXs

C_{ij}	ε-CL-20	PBX A	PBX B	PBX C	PBX D	PBX E	PBX F	PBX G
C_{11}	16.99	9.14	11.45	9.78	9.20	10.39	10.40	9.18
C_{22}	16.96	9.14	10.76	10.02	9.74	10.83	10.26	10.30
C_{33}	25.98	1.58	1.54	1.40	2.93	0.79	5.03	0.78
C_{44}	4.13	1.69	2.26	2.18	1.04	1.08	1.51	2.48
C_{55}	4.93	1.28	2.06	1.76	1.82	0.45	1.94	0.93
C_{66}	7.34	5.42	4.78	5.50	5.55	5.50	6.25	5.09
C_{12}	6.36	4.43	4.37	4.08	4.60	4.73	4.87	4.78
C_{13}	4.68	−0.81	0.31	0.48	0.31	0.30	1.25	0.52
C_{23}	0.13	0.04	0.27	0.51	0.29	0.53	−0.04	−0.50
λ	9.04	1.03	1.84	0.78	1.68	2.65	2.10	1.09
μ	5.47	2.79	3.06	3.14	2.80	2.34	3.23	2.83

$$\begin{bmatrix} \sigma_1 \\ \sigma_2 \\ \sigma_3 \\ \sigma_4 \\ \sigma_5 \\ \sigma_6 \end{bmatrix} = \begin{bmatrix} C_{11} & C_{12} & C_{13} & C_{14} & C_{15} & C_{16} \\ C_{21} & C_{22} & C_{23} & C_{24} & C_{25} & C_{26} \\ C_{31} & C_{32} & C_{33} & C_{34} & C_{35} & C_{36} \\ C_{41} & C_{42} & C_{43} & C_{44} & C_{45} & C_{46} \\ C_{51} & C_{52} & C_{53} & C_{54} & C_{55} & C_{56} \\ C_{61} & C_{62} & C_{63} & C_{64} & C_{65} & C_{66} \end{bmatrix} \begin{bmatrix} \varepsilon_1 \\ \varepsilon_2 \\ \varepsilon_3 \\ \varepsilon_4 \\ \varepsilon_5 \\ \varepsilon_6 \end{bmatrix} \quad (5)$$

In addition, mechanical properties of materials, such as Young's modulus (E), Bulk modulus (K), Shear modulus (G), and Poisson's ratio (γ), can be predicted depending on the λ and μ parameters, and their correlations with materials mechanical properties are displayed in Eq. (6) [49].

$$\begin{aligned} E &= \mu\left(\frac{3\lambda + 2\mu}{\lambda + \mu}\right) \\ K &= \lambda + \frac{2}{3}\mu \\ G &= \mu \\ \gamma &= \frac{\lambda}{2(\lambda + \mu)} \end{aligned} \quad (6)$$

Specific mechanical properties of PBXs were displayed in Table 6 and Fig. 5, it can be found that all mechanical property values have declined comparing with ε-CL-20, except for Cauchy pressure C_{12}-C_{44}. It is also found that the predicted Young's modulus (E) of PBXs considerably decreased compared with that of ε-CL-20, revealing that the rigidity of the PBXs are lower than that of ε-CL-20, namely, these PBXs are more easy to be deformed. The Young's modulus E of the PBXs are in the range of 5.93–7.74 GPa, indicating that the rigidity of these PBXs are close. The Bulk modulus (K) are closely related to the breaking strength of the materials, that is to say, the higher the Bulk modulus is, the harder the breaking strength of the materials is. From Table 6, it can be noted that the values of the Bulk modulus follow the sequence as: 4.26 GPa (PBX F) > 4.21 GPa (PBX E) > 3.87 GPa (PBX B) > 3.55 GPa (PBX D) > 2.98 GPa (PBX G) > 2.90 GPa (PBX A) > 2.87 GPa (PBX C). It indicates that PBX F has the strongest breaking strength, and PBX C has the weakest. As another key parameter, Share modulus (G) reveals the yield strength of the materials, it can be found in Table 6 that PBX F has the highest Share modulus (G) values, and PBX E has the lowest values. As to Share modulus (G), the values of the PBXs are located in the range between the values of PBX E and that of PBX F. Moreover, the ductility of materials can be assessed by both K/G and Cauchy pressure C_{12}-C_{44} methods, the distinction between them is that the former is related to the plastic deformation of the materials, while the latter is based on the morphology fracture surface of the materials. Thus, PBX E and PBX F have relatively higher K/G and Cauchy pressure C_{12}-C_{44} values among all the PBXs, illustrating that they have better ductility on plastic deformation and morphology fracture surface of materials. Conversely, PBX C and PBX G have relatively lower K/G and Cauchy pressure C_{12}-C_{44} values among all the PBXs, demonstrating that they not only have weak plastic deformation, but also easy to fracture on morphology surface. Moreover, for stable, isotropic, linear elastic materials, their generalized Poisson's ratio γ values are in the range of − 0.1 to 0.5 [50]. Table 6 displays the predicted γ of ε-CL-20 and seven PBXs, and all their values are in the range of − 0.1–0.5, confirming that these PBXs are in accordance with the actual situation.

Oxygen balance

Oxygen balance (OB), as one of the key parameters of energetic materials, indicates the combustion performance of energetic materials. According to OB values, energetic materials can be classified into three types viz. abundant oxygen explosives (OB > 0), deficient oxygen explosives (OB < 0), and zero oxygen explosives (OB = 0) [51]. The mono-explosive energetic materials, composed of C, H, O, and N elements and with formula $C_aH_bO_cN_d$, its OB can be calculated by Eq. (7), but it is unsuitable for complex energetic materials such as PBXs or aluminum (Al) contained propellants. Hence, Zhang [52] had proposed a method for calculating OB based on electronegativity of atoms. Equations (8) and (9) both can be used to calculate the OB for complicated energetic explosives, the distinction between these two equations is that the former is based on molecular weight, while the latter is based

Table 6 Predicted mechanical property values of ε-CL-20 and designed PBXs

Content	ε-CL-20	PBX A	PBX B	PBX C	PBX D	PBX E	PBX F	PBX G
E (GPa)	14.34	6.34	7.22	6.91	6.66	5.93	7.74	6.45
K (GPa)	12.69	2.90	3.87	2.87	3.55	4.21	4.26	2.98
G (GPa)	5.47	2.79	3.04	3.14	2.80	2.34	3.23	2.83
K/G	2.32	1.04	1.27	0.91	1.26	1.8	1.32	1.05
γ	0.31	0.13	0.19	0.10	0.19	0.27	0.20	0.14
C_{12}-C_{44}	2.23	2.74	2.11	1.90	3.56	3.65	3.37	2.30

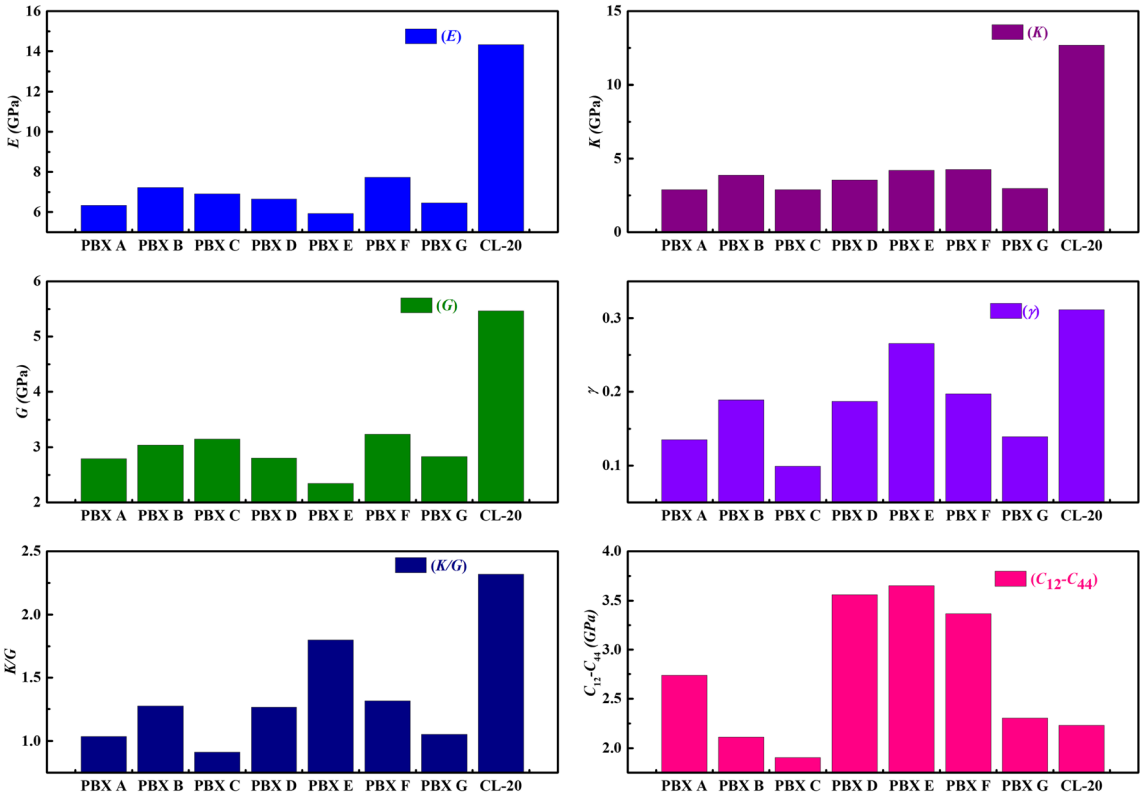

Fig. 5 Comparison of mechanical property of PBXs (A–G) vs ε-CL-20

on the total number of atoms. However, it is believed that the OB of complex energetic materials can be calculated as the sum of each composites OB on multiplications with their corresponding ratios. So, Eqs. (8) and (9) can be further denoted as Eqs. (10) and (11), where OB'_{poly} (OB''_{poly}) and $OB'_{mono\text{-}ex}$ ($OB''_{mono\text{-}ex}$) are OB of the polymer binders and the mono-explosives, respectively, and their values are shown in Table 7.

$$OB = \frac{\left[c-\left(2a+\frac{b}{2}\right)\right]\times 16}{M_r}\times 100\% \quad (7)$$

$$OB' = \frac{800\left(\sum A_{oi}B_{oi}-\sum A_{rj}B_{rj}\right)}{M_r} \quad (8)$$

$$OB'' = \frac{50\left(\sum A_{oi}B_{oi}-\sum A_{rj}B_{rj}\right)}{n} \quad (9)$$

$$OB'^{*} = OB'_{poly}x_i + OB'_{expl}x_j \quad (10)$$

$$OB''^{*} = OB''_{poly}x_i + OB''_{expl}x_j \quad (11)$$

The variables in Eqs. (7)–(11) are defined as:

M_r molecular weight
A_{oi} atom number for *i*th element of the oxidant
A_{rj} atom number for *j*th element of the combustible agent
B_{oi} valance for *i*th element of the oxidant
B_{rj} valance for *j*th element of the combustible agent
n total atom numbers
x_i weight ratio of the polymer binder in PBX
x_j weight ratio of ε-CL-20 in PBX

However, the chemical formula of PBXs is required for further calculation of the OB of PBXs. Herein, we assumed the chemical formula of ε-CL-20 and PBXs (A–G) by using the weight of 1000 g. That is to say, for 1000 g ε-CL-20, the assumed chemical formula can be evaluated as $C_{13.693}H_{13.693}N_{27.388}O_{27.388}$, and the assumed chemical formulas for the PBXs are displayed in Table S1. For PPESKs and ε-CL-20, their assumed chemical formulas are shown in Table S2. Due to the difference of polymer ratios in various PBXs, it is irrational to compare the difference of introduced function groups in PBXs at different ratios. Therefore, polymer ratios for these PBXs need to be normalized. To that end, all polymer ratios of these PBXs are supposed to be 6.8 wt% (based on PBX A) and their assumed chemical formulas also can be found in Table S3. Moreover, based on their assumed chemical formulas, the calculated OB is labeled as OB (6.8 wt%) to distinguish with OB for different polymer ratios in initially designed PBXs in Table 7 and Fig. 6.

From Table 7, it can be seen that the predicted OB′ and OB′* of the PBXs have the same values, showing that Eq. (10) is a simplified equation based on Eq. (8). That is to say, if the OB of mono-explosive, weight ratio of mono-explosive and assumed chemical formula of polymers were acquired, the OB

Table 7 Predicted OB for ε-CL-20 and designed PBXs

Comp.	OB′	OB″	OB′*	OB″*	OB′ (6.8 wt%)	OB″ (6.8 wt%)	OB′* (6.8 wt%)	OB″* (6.8 wt%)
CL-20	− 10.96%	− 8.33%	–	–	–	–	–	–
PBX A	− 24.56%	− 18.24%	− 24.56%	− 15.95%	− 24.53%	− 18.24%	− 24.53%	− 18.40%
PBX B	− 23.61%	− 17.60%	− 23.61%	− 14.88%	− 22.16%	− 16.54%	− 22.16%	− 17.32%
PBX C	− 23.44%	− 17.05%	− 23.44%	− 14.70%	− 21.12%	− 15.85%	− 21.12%	− 17.14%
PBX D	− 24.41%	− 18.13%	− 24.41%	− 15.46%	− 23.86%	− 17.72%	− 23.86%	− 17.91%
PBX E	− 24.93%	− 18.53%	− 24.93%	− 15.14%	− 22.68%	− 16.92%	− 22.68%	− 17.59%
PBX F	− 23.50%	− 17.50%	− 23.50%	− 14.23%	− 20.76%	− 15.53%	− 20.76%	− 16.68%
PBX G	− 23.10%	− 17.33%	− 23.10%	− 14.95%	− 21.28%	− 16.00%	− 21.28%	− 17.40%

of the PBXs could be computed via Eq. (10). Calculated OB of ε-CL-20 by Eq. (7) and Eq. (8) have same values, implying that Eq. (8) also can be utilized for calculating OB for the simple mono-component explosives. Moreover, all the OB values of PBXs computed by Eqs. (8)–(11) are lower than that of pure ε-CL-20, indicating that adding polymers in the ε-CL-20 reduce the OB value of PBXs. In addition, the OB values calculated by Eq. (9) are higher than those calculated by Eq. (8) for the same compound. Same polymer ratio for PBXs are normalized at the ratio (6.8 wt%) to estimate the influence of the OB. It can be seen that OB′ and OB″ values of the PBX A and the PBX D are lower than those of the other PBXs, especially for the PBX F, because the former two PBXs contain much higher hydrogen ratio than other PBXs.

In general, the OB values of the PBXs are lower than that of the ε-CL-20 because the additional polymer binders are added into ε-CL-20. Moreover, the OB values calculated in Eq. (9) are higher than those calculated in Eq. (8), due to reason that the former is calculated from the atom number and valance of element, but the latter takes account of molecular weight. Finally, if the OB values of explosives are getting closer to zero, the explosives are less hazardous to the environment. Comparing these OB values, PBX F has superior OB property among the PBXs.

Detonation performance

The ideal high energetic density materials (HEDMs) are anticipated not only having suitable mechanical properties, appropriate sensitivity, and sufficient high energetic density, but also with better detonation performance; however, it is hard for a HEDM to possess all of these advantages at the same time. As an important parameter for HEDMs, detonation performance is generally utilized for predicting the energetic density of the explosive materials. Moreover, detonation performance is also a significant guidance for designing explosives. Up to now, lots of efforts have been made to predict detonation performance via new methods [53–55]. In this work, we choose the methods which Duan and his co-workers [56] proposed to predict detonation performance in 1992. For mono-explosive, detonation velocity D and detonation pressure P are simple, but composite explosives are more complicated. To calculate D and P values for PBXs, both the

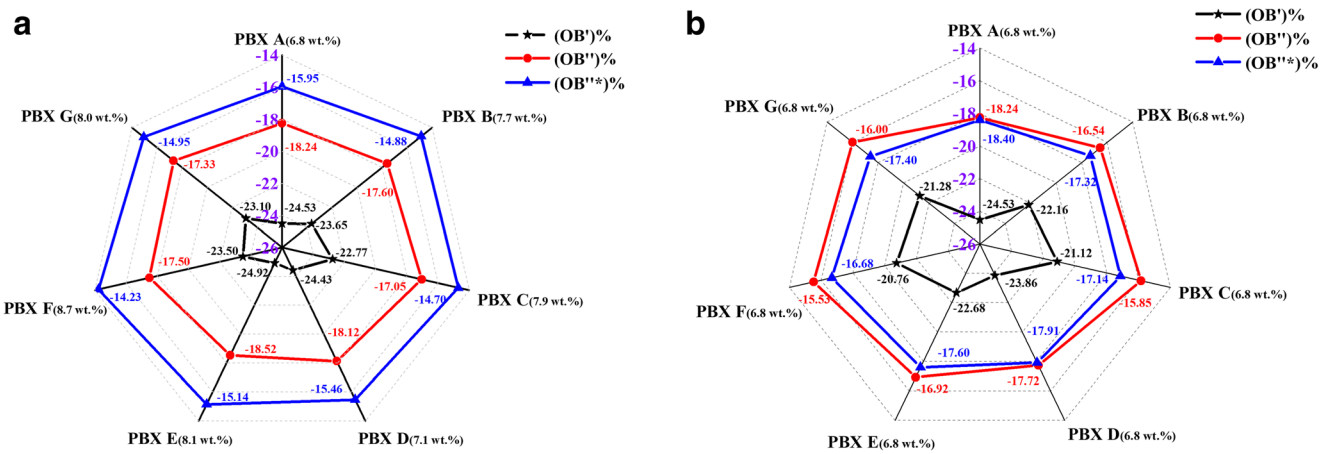

Fig. 6 Predicted OB values for the designed PBXs at specific ratios (**a**) and normalized ratio (6.8 wt%) (**b**)

Table 8 Predicted detonation velocity (D) and detonation pressure (P) of PBXs (A–G)

comp Properties	CL-20	PBX A	PBX B	PBX C	PBX D	PBX E	PBX F	PBX G
x_i		6.8 wt%	7.7 wt%	7.9 wt%	7.1 wt%	8.1 wt%	8.7 wt%	8.0 wt%
ρ(g cm^{-1})	2.01	1.710	1.729	1.733	1.717	1.738	1.748	1.736
ρ*(g cm^{-1})	–	1.941	1.940	1.947	1.939	1.936	1.940	1.949
D'(m s^{-1})	–	9054.04	9017.26	9022.07	9038.48	8993.29	8977.46	9021.36
D''(m s^{-1})	–	8178.60	8218.01	8226.62	8193.69	8236.43	8253.27	8233.95
P'(GPa)	–	36.78	36.05	36.14	36.47	35.57	35.26	36.13
P''(GPa)	–	27.91	28.03	28.14	27.95	28.04	28.08	28.21

Detonation velocity (D) and detonation pressure (P) of the CL-20 are 9460 m s^{-1} and 45.41 GPa, which are cited from the reference [57]

polymers influence and the air influence should be considered and the specific formations are displayed in Eqs. (13)–(14) and (17)–(18). Thus, D and P for composite explosives are regarded as the sum of D and P of the detached components, and can be expressed as:

$$D = \sum D_i \cdot V_i \tag{12}$$

$$D' = D_{poly} + \left(D_{expl} - D_{poly}\right) \cdot \left(\frac{\sum\left(\frac{m_{expl}}{\rho_{expl}}\right)}{\sum\left(\frac{m_i}{\rho_i}\right)} \right) \tag{13}$$

$$D'' = \frac{D'}{4} + \frac{3}{4} \cdot D' \cdot \frac{\rho}{\rho^*} \tag{14}$$

$$\rho^* = \frac{\rho_{expl} \cdot \rho_{poly}}{x_j \rho_{poly} + x_i \rho_{expl}} \tag{15}$$

$$P = \sum \sqrt{P_i} \cdot V_i \tag{16}$$

$$P' = P \left(\frac{\sum\left(\frac{m_{expl}}{\rho_{expl}}\right)}{\sum\left(\frac{m_i}{\rho_i}\right)} \right)^2 \tag{17}$$

$$P'' = P' \cdot \left(\frac{\rho}{\rho^*}\right)^2 \tag{18}$$

In which, the variables from Eqs. (12)–(18) are illustrated and defined as below:

D_i detonation velocity of ith component
V_i volume fraction of ith component
D' detonation velocity of PBX
D_{poly} characteristic velocity of the polymers (value = 5400 m s^{-1}) [56]
D_{expl} detonation velocity of mono-explosive (value = 9460 m s^{-1}) [57]
D'' modified detonation velocity by considering the air influence of PBX
m_{expl} mono-explosive weight of PBX
m_i weight of ith component
ρ_{expl} density of the explosive
ρ_i density of ith component
ρ^* theoretical density of PBX at the specific polymer ratio
ρ density of PBX at the specific polymer ratio
x_i weight ratio of the polymers in PBX
x_j weight ratio of the mono-explosive in PBX
P_i detonation pressure of ith component
P' detonation pressure of PBX
P'' modified detonation pressure by considering the air influence of PBX

From Table 8 and Fig. 7, it can be found that the detonation velocity of all PBXs are about 8300 m s^{-1}, nearly about 85% detonation velocity of the ε-CL-20, indicating that these PBXs still have rather high detonation velocity. Since polymer ratios are different in PBXs, it is improper to compare the detonation velocity for these PBXs. Though, it can be noted that the PBXs with similar ratio of polymers have close detonation velocities, for instance, the detonation velocity difference of PBX G and PBX C (the difference of the polymer ratio is only 0.1 wt%) is within 8 m s^{-1}. Moreover, the differences of the values between D' and D'' of these PBXs are about 800 m s^{-1}, illustrating that the influence of air is much higher than that of various polymers on the detonation velocity. Similarly, the detonation pressure of these PBXs is nearly about 36 GPa, which are about 80% of the detonation pressure of the ε-CL-20; however, the P'' values are much lower than those of the P', and the P'' values of these PBXs are nearly about 60% of ε-CL-20 detonation pressure, indicating that the influence of the air for detonation pressure is greater than those that happened to the polymers for the PBXs.

Sensitivity

The sensitivity is one of the important parameters of the explosives, and it is usually tested by drop-weighttest (h_{50}) [58, 59], which is the height from a given sample mass

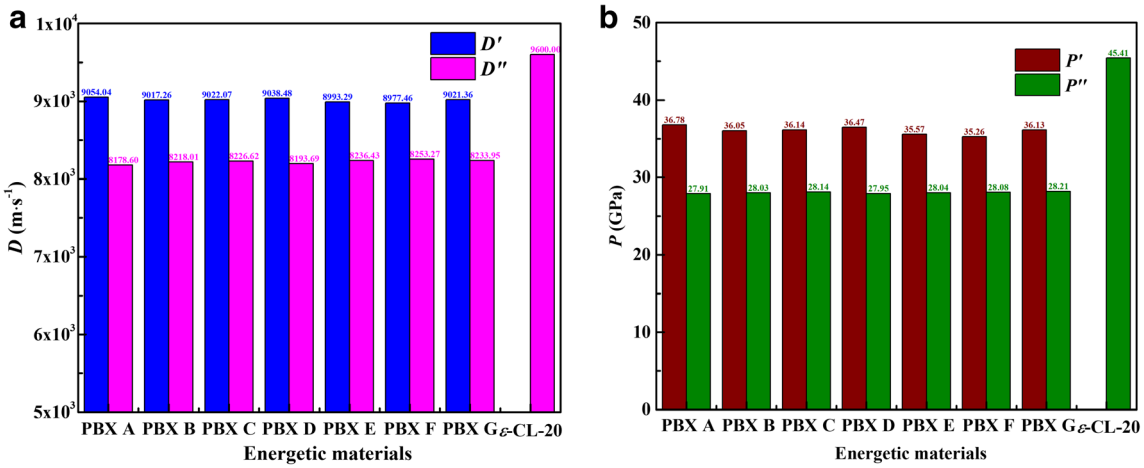

Fig. 7 Predicted detonation velocity (*D*) and detonation pressure (*P*) for PBXs (A–G) and ε-CL-20

dropped upon to make 50% of the time to initiate the reactions of the sample compounds. Moreover, the sensitivity of the explosives can be ascribed to many factors, i.e., maximum detonation heat release [60], free space per molecule in the crystal lattice [61, 62], and strongly positive molecular surface electrostatic potential [63]. These factors are generally appropriate for assessing the sensitivity of mono-explosive or co-crystal explosives. Polizer et al. [64] have systematically discussed the relationship between the performance and the sensitivity for the C,H,O,N, formed mono-explosives, or co-crystal explosives, which can be assessed by their heat formations, free space in the crystal lattice, and strongly positive molecular surface electrostatic potential. However, the seven designed PBXs, unlike the mono-explosive or co-crystal explosives which have the specific molecular format, the moral ratio and the heat formations, are complex systems consisted of the polymer binders and explosives. Hence, the sensitivity of the PBXs is hard to be assessed accurately at the present time. But, in our work mentioned above, the length of the N-NO_2 can be roughly used as a reference to judge the sensitivity of the PBXs. In these PBXs, the PBX C has the largest N-NO_2 length (1.43 Å), with that the PBX B and the PBX D have higher N-NO_2 length (1.40 Å) than those of other four PBXs (N-NO_2 length (1.39 Å)) (PBX A, PBX E, PBX F, and PBX G).

Conclusions

In this work, we have studied the binding energies and the mechanical properties of PPESK (A-G)/ε-CL-20 PBXs via MD simulations. OB and detonation properties of these PBXs have been predicted based on those of ε-CL-20. Effects of various PPESKs (A-G) on the (0 0 1) crystal surfaces of ε-CL-20 have been investigated, and the specific findings are generalized as follows:

(1) The CED and δ of seven PBXs (A–G) have been predicted with the order of PBX F > PBX D > PBX A > PBX E > PBX B > PBX C > PBX G via their specific values.
(2) The pyrolytic trigger bond N-NO_2 of PBX C is 1.49 Å at 298 K, which is higher than those of other PBXs, indicating that PBX C is less stable than other PBXs at ambient temperature.
(3) The binding energies between PPESKs (A–G) and ε-CL-20 are obtained with the sequence of PBX E > PBX F > PBX D > PBX A > PBX G > PBX B > PBX C.
(4) The RDF results of PBXs (A–G) indicate that both hydrogen and van der Waals interactions exist between polymers and ε-CL-20.
(5) The mechanical properties of PBXs (A–G) have been predicted and are compared with those of the pure ε-CL-20. The results imply that the mechanical properties are improved by adding the polymer binders; however, PBX C and PBX G have low *K*/*G* and C_{12}-C_{44} values, demonstrating that these two PBXs have weaker ductility among the PBXs, and it is contrary to PBX E and PBX F.
(6) OB have been calculated for these PBXs. The results indicate that all PBXs' OB are lower than that of the pure ε-CL-20. OB values have also been predicted for the PBXs (A–G) at same polymer ratios (6.8 wt%), and in which PBX F has the highest OB values among the PBXs.
(7) Detonation properties for these PBXs have been predicted, in which *D* of these PBXs are at about 9000 m s^{-1} and *P* of these PBXs are nearly at 36 GPa, the detonation properties of these PBXs are less influenced by different polymer binders. For these seven PBXs, PBX C has the lowest sensitivity among the PBXs.

In general, the MD simulations on ε-CL-20 and PPESKs (A–G)/ε-CL-20 PBXs provide much information for their

binding energies, CED, δ, mechanical properties, oxygen balance, and detonation properties. These may not only be utilized for filtering the energetic polymer binders, but also help for guiding the composite design for the PBXs.

Funding information Authors appreciate the financial support from the National Natural Science Foundation of China (grant nos. 21673018 and 21703168), Science and Technology Program of Guangzhou (2016201604030043, China), and Sichuan University of Science and Engineering (2017RCL44).

Compliance with ethical standards

Conflicts of interest The authors declare that they have no conflict of interest.

Publisher's Note Springer Nature remains neutral with regard to jurisdictional claims in published maps and institutional affiliations.

References

1. Shu YJ, Huo JC (2011) Theory of explosives. Chemical Industry, Beijing
2. Ou YX, Liu JQ (2005) High energy density compounds. National Defense Industry, Beijing
3. Klapöke TM (2007) High energy density materials. Springer-Verlag, Berlin
4. Foltz MF (1994) Thermal stability of ε-hexanitrohexaazaisowurtzitane in an estane formulation. Propell Explos Pyrot 19:63–69
5. Foltz MF, Coon CL, Garcia F, Nichols III AL (1994) The thermal stability of the polymorphs of hexanitrohexaazaisowurtzitane, part II. Propell Explos Pyrot 19:133–144
6. Wang Y, Song XL, Song D, Jiang W, Liu HY, Li FS (2013) A versatile methodology using sol-gel, supercritical extraction, and etching to fabricate a nitramine explosive: nanometer HNIW. J Energ Mater 31:49–59
7. Li J, Brill TM (2007) Kinetics of solid polymorphic phase transitions of CL-20. Propell Explos Pyrot 32(4):326–330
8. Simpson RL, Urtiew PA, Ornellas DL, Moody GL, Scribner KJ, Hoffman DM (1997) CL-20 performance exceeds that of HMX and its sensitivity is moderate. Propell Explos Pyrot 22:249–255
9. Ghosh M, Venkatesan V, Mandav S, Banerjee S, Sikder N, Sikder AK, Bhattacharya B (2014) Probing crystal growth of ε- and α-CL-20 polymorphs via metastable phase transition using microscopy and vibrational spectroscopy. Cryst Growth Des 14:5053–5063
10. Wei XF, Xu JJ, Li HZ, Long XP, Zhang CY (2016) Comparative study of experiments and calculations on the polymorphisms of 2,4,6,8,10,12-hexanitro-2,4,6,8,10,12-hexaazaisowurtzitane (CL-20) precipitated by solvent/antisolvent method. J Phys Chem C 120:5042–5051
11. Millar DIA, Maynard-Casely HE, Kleppe AK, Marshall WG, Pulham CR, Cumming AS (2010) Putting the squeeze on energetic materials-structural characterization of a high-pressure phase of CL-20. Cryst Eng Comm 12:2524–2527
12. Zhao XQ, Shi NC (1995) Crystal structure of ε-hexanitrohexaa zaisowurtzitane. Chin Sci Bull 40:2158–2160
13. Bolton O, Matzger AJ (2011) Improved stability and smart-material functionality realized in an energetic cocrystal. Angew Chem Int Ed 50:8960–8963
14. Doblas D, Rosenthal M, Burghammer M, Chernyshov D, Spitzer D, Ivanov DA (2016) Smart energetic nanosized co-crystals: exploring fast structure formation and decomposition. Cryst Growth Des 16:432−439
15. Yan QL, Zeman S,Zhao FQ, Elbeih A (2013) Non-isothermal analysis of C4 bonded explosives containing different cyclic nitramines. Thermochim Acta 556:6−12
16. Yan QL, Zeman S, Elbeih A (2013) Thermal behavior and decomposition kinetics of viton A bonded explosives containing attractive cyclic nitramines. Thermochim Acta 562:56−64
17. Yan QL, Zeman S, Zhang TL, Elbeih A (2013) Non-isothermal decomposition behavior of fluorel bonded explosives containing attractive cyclic nitramines. Thermochim Acta 574:10−18
18. Li HR, Shu YJ, Gao SJ, Chen L, Ma Q, Ju XH (2013) Easy methods to study the smart energetic TNT/CL-20 co-crystal. J Mol Model 19:4909–4917
19. Sun T, Liu Q,Xiao JJ, Zhao F, Xiao HM (2014) Molecular dynamics simulation of interface interactions and mechanical properties of CL-20/HMX cocrystal and its based PBXs. Acta Chim Sinica 72:1036–1042
20. Han G, Li QF, Gou RJ, Zhang SH, Ren FD, Guan R(2017) Growth morphology of CL-20/HMX cocrystal explosive: insights from solvent behavior under different temperatures. J Mol Model 23:360
21. Wu ZK, Shu YJ et al. (2016) Molecular dynamics simulation of CL-20/FOX-7 co-crystal. insights from solvent behavior under different temperatures. Chin J Expl Propell 39(3):37–42
22. Zhu SF, Zhang SH, Gou RJ, Han G, Wu CL (2017) Theoretical investigation of the effects of the molar ratio and solvent on the formation of the pyrazole–nitroamine cocrystal explosive 3,4-dinitropyrazole (DNP)/2,4,6,8,10,12-hexanitrohexaazaisowurtzitane (CL-20). J Mol Model 23:353
23. Asay BW (2009) Non-Shock initiation of explosives. Springer, Berlin
24. Lundberg AW (1996) High Explosives in stockpile surveillance indicate constancy. Science & Technology Review (December):13–17
25. Zeman S, Elbeih A,Yan QL (2013) Note on the use of the vacuum stability test in the study of initiation reactivity of attractive cyclic nitramines in the P1 Matrix. J Therm Anal Calorim 111:1503−1506
26. Zeman S, Elbeih A, Yan QL (2013) Note on the use of the vacuum stability test in the study of initiation reactivity of attractive cyclic nitramines in the C4 Matrix. J Therm Anal Calorim 112:433−1437
27. Yuan LL, Xiao JJ, Zhao F, Xiao HM (2016) Molecular dynamics simulation of composites formed with e-CL-20 and PVA, PEG on different crystalline surfaces. Chin J Energ Mater 2:124–128
28. Tao J, Wang XF,Zhao SX, Wang CL, Diao XQ, Han ZX (2015) Simulation and calculation for binding energy and mechanical properties of e-CL-20/energetic polymer binder mixed system. Chin J Energ Mater 4:315–322
29. Wang JY, Jian XG (2016) Applications of high performance phthalazinone-containing pesins in insulating materials. Insulating Materials 49(10):17–23
30. Liu C, Jian XG (2011) Recent progress in thermoplastic composites based on poly(aryl ether)s containing phthalazinone moiety. Chin Polym Bull 9:52–62
31. Jian XG, Liao GX, Wang JY (2002) Research progress of poly-(arylene ether ketone)s and poly(arylene ether sulfone)s containing phthalazinone moieties. China Plastics 16:11–15
32. Wang JY, Jian XG (2011) Progress on synthesis of heterocyclic polymers containing phthalazinone moiety and the relationship of their structure and properties. Chin Polym Bull 9:22–34
33. Wang K, Shu YJ et al. (2017) Molecular dynamics simulations for performance of PPESK and PPESK/ε-CL-20 composite system. Chin J Expl Propell 40(4):38–43
34. Shu Y, Wang DT et al. (2018) Molecular dynamics simulation on the physical properties of the novel designed poly-(phthalazinone ether sulfone ketone) (PPESK). Comp Mater Sci 152:158–164

35. Shu Y, Yi Y et al. (2017) Interactions between poly-(phthalazinone ether sulfone ketone) (PPESK) and TNT or TATB in polymer bonded explosives: a molecular dynamic simulation study. J Mol Model 23:334
36. Xu XJ, Xiao HM, Xiao JJ, Zhu W, Huang H, Li JS (2006) Molecular dynamics simulations for pure ε-CL20 and ε-CL20-based PBXs. J Phys Chem B 110:7203–7207
37. Accelrys Software Inc Materials Studio Accelrys Software Inc San Diego
38. Akkermans RLC, Spenley NA, Robertson SH (2013) Monte Carlo codes, tools and algorithms Monte Carlo methods in materials studio. Mol Simulat 39:1153–1164
39. Andersen HC (1980) Molecular dynamics simulations at constant pressure and /or temperature. J Chem Phys 72:2384–2393
40. Berendsen HJC, Postma JPM, Gunsteren WF, DiNola A, Haak JR (1984) Molecular dynamics with coupling to an external bath. J Chem Phys 81:3684–3690
41. Allen MP, Tildesley DJ (1983) Computer simulation of liquids. Oxford University Press, Oxford
42. Sun H (1998) COMPASS: an ab initio force-field optimized for condensed-phase applications overview with details on alkane and benzene compounds. J Phys Chem B 102:7338–7364
43. Liu N, Zeman S, Shu YJ, Wu ZK, Wang BZ, Shi WY (2016) Comparative study of melting points of 3,4-bis(3-nitrofurazan-4-yl)furoxan (DNTF)/1,3,3-trinitroazetidine (TNAZ) eutectic compositions using molecular dynamic simulations. RSC Adv 6:59141–59149
44. Lu YY, Shu YJ et al. (2018) Molecular dynamics simulations on ε-CL-20-based PBXs with added GAP and its derivative polymers. RSC Adv 8:4955–4962
45. Abboud JLM, Notario R (1999) Critical compilation of scales of solvent parameters. Part I. pure, non-hydrogen bond donor solvents-technical report. Pure Appl Chem 71:645–718
46. Xu XJ, Xiao HM, Ju XH, Gong XD (2005) Theoretical study on pyrolysis mechanism for ε-hexanitrohexaazaisowurtzitane. Chin J Org Chem 5:536–539
47. Qiu L, Zhu WH, Xiao JJ, Zhu W, Xiao HM, Huang H, Li JS (2007) Molecular dynamics simulations of trans-1,4,5,8-tetranitro-1,4,5,8-tetraazadecalin-based polymer-bonded explosives. J Phys Chem B 111:1559–1566
48. Watt JP, Davies GF, O'Connell RJ (1976) The elastic properties of composite materials. Rev Geophys Space Phys 14:541–563
49. Weiner JH, Milstein F (1983) Statistical mechanics of elasticity. Wiley, New York
50. Landau LD, Lifshitz EM (1986) Theory of elasticity. Pergamon, Oxford
51. Rudolf M, Köhler J, Homburg DIA (2007) Explosives, 6th Ed. Wiley-VCH, Weinheim
52. Zhang HS (1982) Oxygen balance of the organic elements explosives. Acta Armamentarh 2:61–63
53. Wu X (1985) Simple method for calculating detonation parameters of explosives. Chin J Energ Mater 3:263–277
54. Kamlet MJ, Jacobs SJ (1968) Chemistry of detonations I. A simple method for calculating detonation properties of C-H-N-O explosives. J Chem Phys 48:23–35
55. Keshavarz MH, Motamedoshariati H, Moghayadnia R, Nazari HR, Azarniamehraban J (2009) A new computer code to evaluate detonation performance of high explosives and their thermochemical properties, part I. J Hazard Mater 172:1218–1228
56. Duan M, Xu GG, Wang YZ (1992) The detonation model and calculation of mixed explosives. Blasting 1:26–28
57. Hang GY, Yu WL, Wang T, Wang JT, Li Z (2017) Theoretical insights into the effects of molar ratios on stabilities, mechanical properties, and detonation performance of CL-20/HMX cocrystal explosives by molecular dynamics simulation. J Mol Model 23:30
58. Zeman S (2007) Sensitivities of high energy compounds. Struct Bonding 125:195–271
59. Storm CB, Stine JR, Kramer JF (1990) Sensitivity relationships in energetic materials, chemistry and physics of energetic materials. Kluwer, Dordrecht
60. Pepekin VI, Korsunskii BL, Denisaev AA (2008) Initiation of solid explosives by mechanical impact. Combust Explos Shock Waves 44:586–590
61. Pospišil M, Vavra P, Concha MC, Murray JS, Politzer P (2011) Sensitivity and the available free space per molecule in the unit cell. J Mol Model 17:2569–2574
62. Politzer P, Murray JS (2014) Impact sensitivity and crystal lattice compressibility/free space. J Mol Model 20:2223
63. Murray JS, Lane P, Politzer P (1998) Effects of strongly electron-attracting components on molecular surface electrostatic potentials: application to predicting impact sensitivities of energetic molecules. Mol Phys 93:187–194
64. Politzer P, Murray JS (2016) High performance, low sensitivity: conflicting or compatible? Propell Explos Pyrot 41:414–425